Hindawi
Advances in Materials Science and Engineering
Volume 2018, Article ID 3246371, 11 pages
https://doi.org/10.1155/2018/3246371

Research Article

Behaviors of Oxide Film during Semisolid Brazing of SiC_p/6063Al Composite Materials

Jing Xiao,[1] **Shun Li**,[1] **Shuxin Bai**,[1] **Jiuchun Yan**,[2] **and Degan Xiong**[1]

[1]*Department of Materials Science and Engineering, National University of Defense Technology, Changsha 410073, China*
[2]*State Key Laboratory of Advanced Welding and Joining, Harbin Institute of Technology, Harbin 150001, China*

Correspondence should be addressed to Shuxin Bai; 13272093806@163.com

Received 6 May 2018; Revised 9 July 2018; Accepted 24 July 2018; Published 2 September 2018

Academic Editor: Xinquan Zhang

The semisolid brazing of SiC_p/6063Al under an applied pressure using Zn-Al-Cu filler metal was investigated. The samples to be joined were heated from 380°C to 382°C, 386°C, 392°C, and 410°C under a constant pressure of 10 MPa, respectively. Effects of the temperature on microstructural evolution and deformation behavior of the filler metal, interfacial structure, and shear strength of the bonded joint were discussed, and the disruption behavior of the surface oxide film was studied. The results show that, after heating, the solid grains of the filler metal transform into a globular structure surrounded by liquid. The degree of sphericity and the liquid fraction tend to improve with increasing temperature. During the heating process, the deformation of the filler metal is first accomplished by plastic deformation of solid grains and then by intergrain sliding and liquid flow. The surface oxides are broken and stripped by a cocontribution of compressive and shear stress which is caused by depressing and sliding of solid grains along the composites. It is found that the heating of 380°C to 392°C under pressure is the optimum condition to disrupt the surface oxide films and obtain sound bonds. The mechanical test results show that the maximum shear strength of the bond joints is as high as 105 MPa, reaching 78% that of the parent materials.

1. Introduction

High volume fraction SiC-reinforced aluminum metal matrix composites (Al-MMCs) is considered as an ideal electronic packaging material due to its attractive properties (e.g., high thermal conductivity, low tunable coefficient of thermal expansion, high modulus, and low density). The associated welding technologies thus attract intense attentions. Among the current joining methods for Al-MMCs, brazing is a competitive candidate because of its flexibility, reliability, and low bonding temperature. However, the presence of the surface oxides is the main barrier to successful bonding. Therefore, conventional brazing methods are normally conducted in vacuum [1, 2] or with flux to reduce the high-temperature oxidation of the faying surfaces. However, joining processes in vacuum increase the overall bonding time and reduce the design flexibility of the parts to be joined; besides, the residual flux is hard to be removed, which could result in a severe corrosive problem. Therefore, the vacuum-free bonding processes which are assisted by physical energy to remove the oxides have been developed increasingly.

Ultrasonic brazing is an elegant method to join Al-MMCs in air with the physical assistance. Due to the cavitation effect caused by the ultrasonic wave, not only the surface oxides are disrupted but also the wettability is enhanced [3–9]. However, higher ultrasonic wave energy may aggravate dissolution of the base metal, which leads to degradation of the substrate properties [10].

Semisolid joining techniques have been developed recently based on semisolid metal processing. The results show that the bonding of the substrate could be realized using the semisolid joining technique with constant pressure. Kiuchi et al. first performed semisolid joining for the aluminum alloy with glass or stone and confirmed the excellent joining ability of the semisolid alloys [11]. Cheng and Zhang [12] carried out semisolid joining for SiC_p/2024Al composites and the 2024 aluminum alloy under high pressure. The bond

strength was increased due to the fine microstructure which arose from the spherical semisolid billet. To overcome the oxide problem and improve the bond interface structure, the semisolid joining technique with motion energy has been recently developed. Narimannezhad et al. [13] and Hosseini et al. [14, 15] developed semisolid stirring joining in the zinc alloy and AZ91 magnesium alloy, respectively. Ideal and nonlinear bond interface were observed under the action of stirring. Yan et al. [16] and Xu et al. [17, 18] carried out semisolid brazing of SiC_p/A356 composites with the assistance of vibration and stirring, respectively. It was found that the mechanical assistance aids the disruption of the oxide films. However, the current methods are often relatively complicated to operate and usually involved with the porosity and crack problem in the joining region [19, 20]. What is more, the intermechanisms including the disruption mechanism of the surface oxides in the processes are not clear.

In this work, a semisolid brazing of SiC_p/6063Al composites under applied pressure was investigated, aiming at simplifying the operation, lowering the cost, and retaining the potential of the semisolid joining. Effects of the brazing temperature on the interfacial structure and shear strength of the joint were probed. Additionally, the disruption behavior of the surface oxide film was also studied by analyzing the microstructural evolution and deformation behavior of the filler metal during the brazing process.

2. Materials and Methods

2.1. Materials. The base materials used in this work were the 6063Al alloy that was reinforced with 63 vol.% SiC particles with a diameter range of 10–100 μm. The materials were produced by vacuum pressure infiltration with shear strength of ~135 MPa at room temperature. The filler metals used in this work were Zn-Al-Cu alloys, whose chemical composition and solidus (T_S) and liquidus (T_L) temperatures are shown in Table 1. Before joining, as-cast Zn-Al-Cu alloys were homogenized at 350°C for 12 h and rolled at 300°C from 30 mm to a thickness of 0.3 mm trip (99% reduction) in several passes. The base materials and filler metal were processed into plates with dimensions of 30 mm × 30 mm × 3 mm and 30 mm × 30 mm × 0.3, respectively. All samples were mechanically polished to a 600-grit finish and then ultrasonically degreased in acetone prior to heating.

2.2. Brazing Process. The filler metal was preset between the base materials. The thermocouple used to measure the temperature was fixed near the bonding line, and an accuracy of the temperature control was ±1°C.

The specimens were heated up to 380°C (T_S) at a heating rate of 20°C·min^{-1} and held for 10 min to homogenize the samples. Then, an axial pressure of 10 MPa was imposed on the upper specimen. Afterwards, the specimens were further heated to four different temperatures of 382, 386, 392, and 410°C at a low rate of 0.5°C·min^{-1} with the pressure, held at the corresponding temperature for 5 min and then cooled down to 200°C at a rate of 5°C·min^{-1}. To ensure adequate solidification of the filler metal, the loading pressure was not removed until the temperature went down to 200°C. The whole brazing process as described in Figure 1 was conducted under argon atmosphere.

2.3. Characterization Test and Observation. To investigate the effect of temperature on the microstructure of the filler metal, the filler metals with dimensions of 30 mm × 30 mm × 0.3 mm were heated to 382°C–410°C without compression and with compression between two SiC_p/Al composites plates (similar to brazing in a furnace), respectively. Then, the specimens were quickly quenched with water.

The filler metals and cross sections of the bonded joints were etched with a 2% solution of nitric acid after mechanical grinding and polishing with 0.5 μm diamond paste. The microstructures were examined by HIROX 200 optical microscope (OM) and SIRION-type field emitting scanning electron microscope (SEM) produced by Japan FEI Corporation. The chemical composition was examined by energy dispersive spectroscopy (EDS). The average grain size, shape factor, and the liquid volume fraction were measured using Leica Q550MW image analysis software. The shear strength tests of the brazed joints were evaluated on the WDW-100 electromechanical universal testing machine with a constant speed of 0.5 mm·min^{-1} at room temperature. In order to guarantee the reliability, a designed jig was applied for the test, as shown in Figure 2(a). In particular, a notch with specific dimension was created on the top of the specimen beside the bond line (a distance of 0.15 mm from the bond line as shown in Figure 2(b)) to accommodate the load. At least five independent tests were conducted under each experiment condition.

3. Results and Discussion

3.1. Effect of Temperature on the Interfacial Structure of the Joint. The interfacial structure of the joint brazed at different temperatures is shown in Figure 3. A continuous oxide film is observed at the interface at 382°C, and a slight zinc diffusion layer appears at the side of the base material (as shown by arrow in Figure 3(a)). As reported by Xu et al. [3], there exist many fractures in the oxide inclusion zone, and zinc is inclined to diffuse into the matrix through the fractures to form a penetration zone. At 386°C, the oxide layer becomes discontinuous and a wider diffusion layer is formed in the composites side (Figure 3(b)). When heated to 392°C, it can be found that the oxide films were broken into small fragments, and a sharply increasing diffusion layer is observed (Figure 3(c)). However, with further increasing of temperature, no visible removal of the oxide layer is obtained. Discrete oxide films are still contained at the bond line, despite the metallic bonding between them (Figure 3(d)).

3.2. Microstructure Evolution and Deformation Behavior of the Filler Metal. The disruption of the surface oxide film

Table 1: Chemical composition and solidus (T_S) and liquidus temperatures (T_L) of the filler metals.

Composition (wt.%)			Solidus and liquidus temperature (°C)	
Zn	Al	Cu	T_S	T_L
Balance	12	4.5	380	420

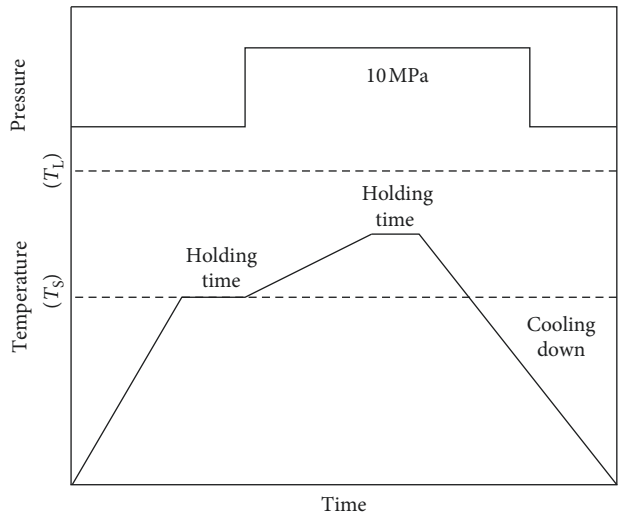

Figure 1: Schematic diagram of the brazing process.

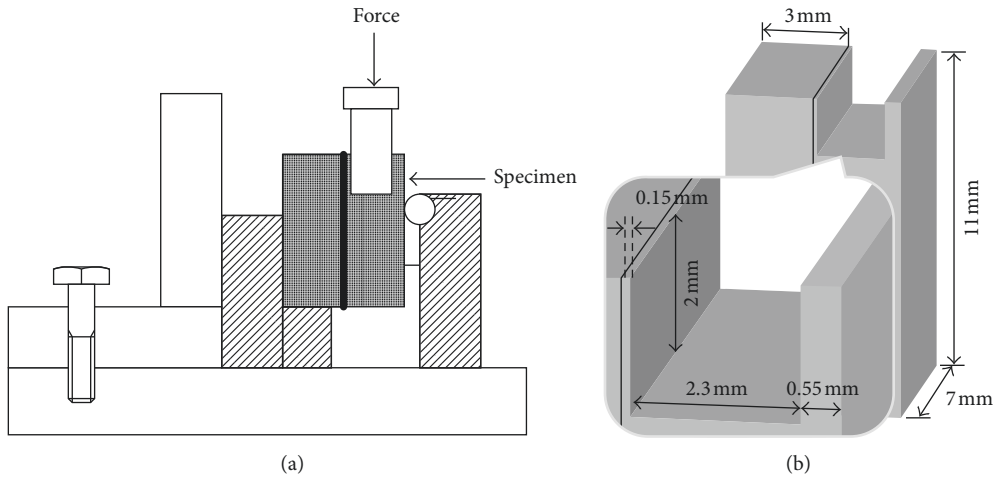

Figure 2: Schematic diagram of (a) shear test arrangement and (b) dimension of the shear specimen (bond line is shown by a thick line).

during the brazing process is considered to be related to the microstructure, compression behavior of the filler metal, and the behavior against the base metal. Therefore, it is very important to verify the microstructural evolution and compression behavior of the filler metal during the heating process. The microstructure of the as-rolled Zn-Al-Cu alloy is shown in Figure 4.

Optical micrograph shows that the microstructure consists of plastically deformed grains aligned in the rolling direction. The backscattered electron image and spot analysis as shown in Table 2 reveal that the microstructure of the Zn-Al-Cu alloy consists of the proeutectic β phase (marked "A"), aluminum-rich α phase (marked "B"), and Zn-rich η phase (marked "C"). Copper additions less than 5% had no significant effect on the microstructure of this alloy. During solidification of the Zn-Al-Cu alloy, proeutectic β forms first and the remaining liquid transforms into the $\beta + \eta$ mixture by the eutectic reaction. During cooling to room temperature, the proeutectic and eutectic β phases both decompose into an alternating layer of α and η [21]. Due to the rolling process, all grains orient themselves in the rolling direction.

The microstructure of the as-rolled Zn-Al-Cu alloy filler metal heated to different temperatures without compression is shown in Figures 5(a)–5(d). It can be seen that no obvious

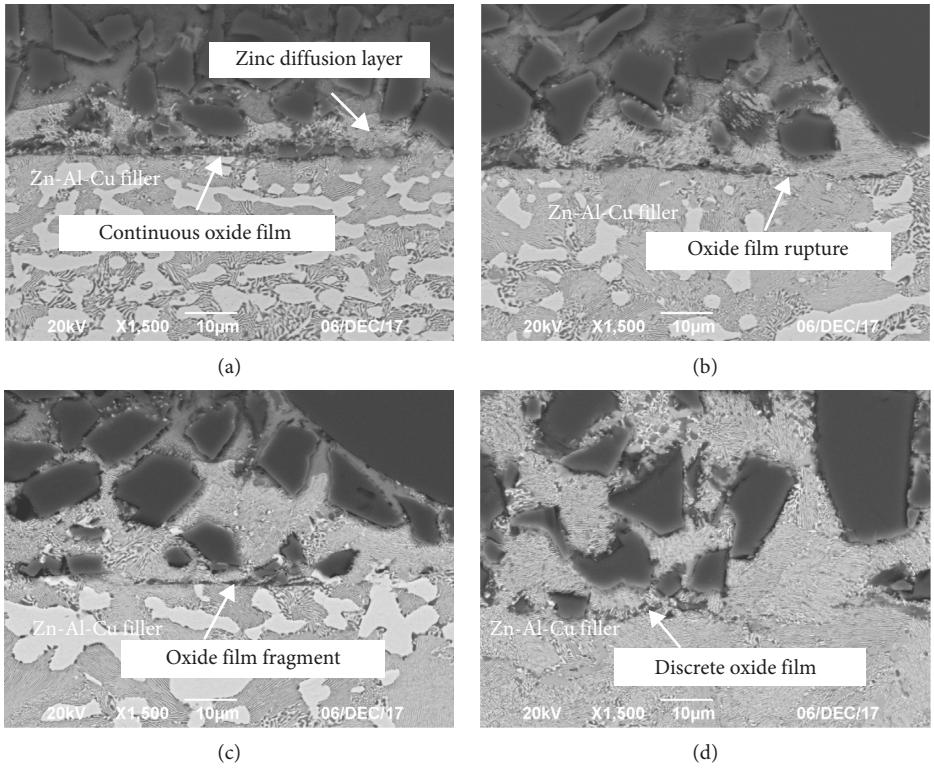

Figure 3: The interfacial structure of the joint brazed at different temperatures: (a) 382°C; (b) 386°C; (c) 392°C; (d) 410°C.

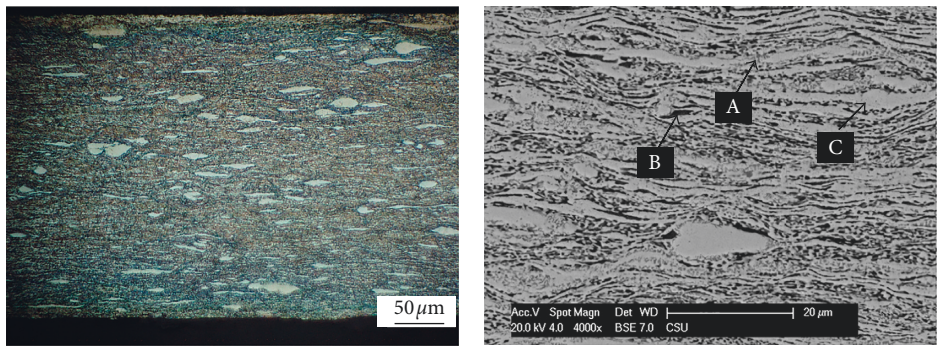

Figure 4: Microstructure of the as-rolled Zn-Al-Cu alloy: (a) optical micrograph; (b) backscattered electron image.

Table 2: EDS analysis results of regions A, B, and C in Figure 4.

Region	Zn	Al	Cu
A	73.31	23.58	3.11
B	61.15	36.86	1.97
C	84.43	1.38	14.19

change can be observed in the microstructure of the Zn-Al-Cu alloy after being heated to 382°C as shown in Figure 5(a). When heated to 386°C, both deformed η-Zn grains and β-Al grains have transformed to near-spherical grains with local liquid at the grain boundary (Figure 5(b)). With the increase of the temperature, most of the η-Zn and β-Al grains become more spheroidal and uniformly distributed in a liquid matrix as shown in Figure 5(c). When the temperature increases to 410°C, coalescence occurs between the adjoining grains and liquid pool forms due to the increasing liquid fraction (Figure 5(d)).

It can also be found that the amount of η-Zn grains tends to decrease with increasing temperature from 382°C to 410°C and they almost disappear after being heated to 410°C.

Figure 6 shows the variation in the shape factor of the solid grains and the liquid fraction as a function of the temperature. As shown in Figure 6, the shape factor increases to a maximum at 392°C and then decreases slightly with further increasing temperature. The liquid fraction measure implies that the liquid fraction is relatively low at

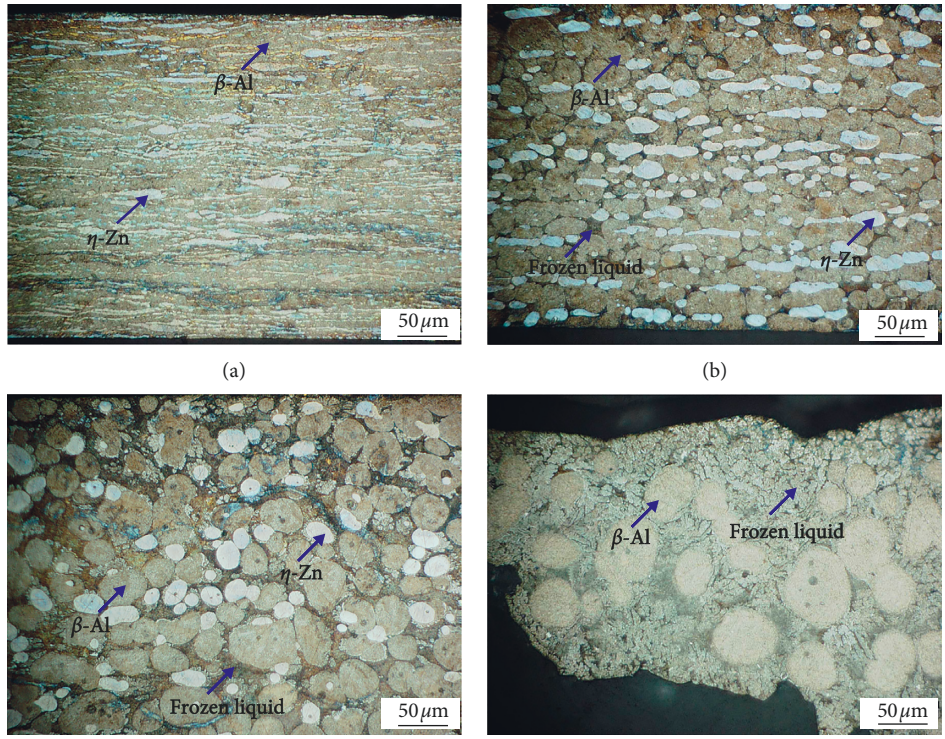

Figure 5: The microstructure of the filler metal heated to different temperatures without compression: (a) 382°C; (b) 386°C; (c) 392°C; (d) 410°C.

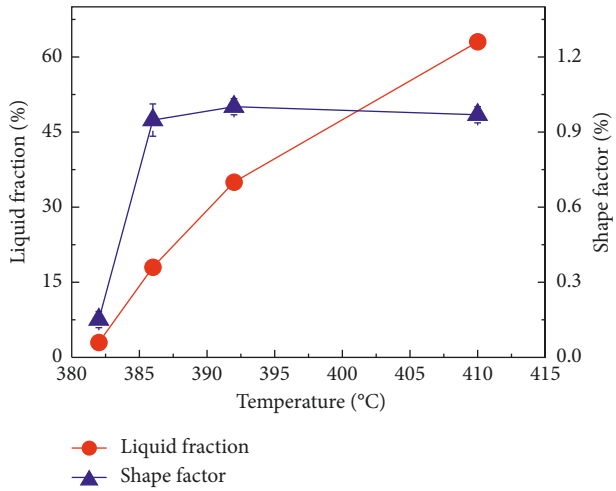

Figure 6: The variation in the shape factor of the solid grains and the liquid fraction as a function of the temperature.

382°C ($f_L = 3\%$), and it increases markedly with increasing temperature.

It is well known that the plastic deformation of the alloy supplied by hot or cold work ultimately results in sufficient stored strain energy. The strain energy then activates the recrystallization and spheroidization of the solid grains during the reheating process [22–25]. Recrystallization is diffusion controlled, and sufficient temperature is thus necessary for diffusion. At temperature below 386°C, thermal energy for recrystallization is insufficient, and recrystallization is thus difficult to be induced. Therefore, there seems to be no detectable recrystal grain appearing in the microstructure at 382°C, as shown in Figure 5(a). With the increase of the temperature, the diffusion rate increases and hence, recrystal grains are able to formed, as illustrated in Figure 5(b). These recrystal grains are, however, partial spheroidal. By continuing the heating process, the grains spheroidize and coarsen due to the minimum interface energy principle. However, spheroidization and coarsening are codominant and compete with each other. During the heating period of 382°C to 392°C, small grains which have a lower melting point are melted in favor of the larger grains and the number is reduced. This process is less effective in particle growth but has a great influence on the spheroidization of solid grains [26], so the shape factor of the solid grains increase obviously in this stage, as shown in Figure 6. During the heating period of 392°C to 410°C, the majority of the solid grains have gained uniform surface curvature, and then growth of spherical grains commences. Hence, obvious coarsening of the grains and decrease of the shape factor are observed as shown in Figures 5 and 6. In addition, according to Figures 5 and 6, it is seen that the increase of the temperature results in the increase of the liquid fraction and the decrease of the number of the η-Zn phase. It is known that when temperature is higher than the eutectic temperature, intergranular eutectic phases ($\alpha + \eta$) melt first to form liquid. This induces a thin liquid layer at the grain boundaries and a little decrease of the η-Zn phase as shown in Figure 5(b).

With the increase of the temperature, large η-Zn particles start to melt, resulting from their low melting point. The higher the temperature, the more the melting of the η-Zn particles, and consequently, the higher the liquid fraction.

Figures 7(a)–7(d) shows the microstructure of the as-rolled Zn-Al-Cu samples heated to different temperatures with compression. The microstructure which underwent both thermal and thermal-compression treatment is somewhat different to that without compression. Firstly, by comparing Figures 5 and 7, β-Al grains in all thermal-compression microstructure have no obvious change, but the grain size and roundness of the η-Zn phase tend to decrease in all conditions. The variation of grain size and roundness of the η-Zn phase with different microstructures is shown in Figure 8. It can be seen that the grain size and roundness of the η-Zn phase in the noncompression microstructure are always higher than that in the thermal-compression microstructure. Moreover, the grain size of η-Zn grains in the noncompression microstructure increases apparently with increasing temperature. However, the trend in the thermal-compression microstructure is quite the reverse (Figure 8(a)). Secondly, the thermal-compression microstructure at the center region is similar to that at the edge region at 382°C as shown in Figures 7(a_1) and 7(a_2). With the increase of the temperature, it can be seen that strong compression makes the liquid squeeze out, which shows a lower fraction of the liquid in the center and higher fraction in the edge (Figures 7(b)–7(d)). Thirdly, the thickness of the filler in the thermal-compression microstructure decreases apparently with increasing temperature. As shown in Figure 7, the thickness of the filler metal is around 290 μm at 382°C, which is a little lower than the initial thickness of the filler metal. As temperature increased from 382°C to 392°C and deformation proceeded, the thickness decreases obviously from 290 μm to around 85 μm. Finally, the interface structure between the filler metal and composites improves with increasing temperature. Unjointed gaps are observed on the interface at 382°C, which is probably due to no disruption of the oxide film in this region and huge residual thermal stress resulted from quenching. The gaps disappear at 386°C, and metallurgical bonding is achieved at 392°C and 410°C, as shown by arrows in Figures 7(c_1) and 7(d_1).

It is well known that the high temperature strength of metals is related to the diffusion ability of metal atoms. The lower the diffusion ability is, the greater the high temperature strength will be. On the contrary, the higher the melting point of metal, the stronger the bonding force of metal atoms and, consequently, the lower the diffusion coefficient of the atoms. In this case, η-Zn grains with the lower melting point will have a lower strength at the elevated temperature. The grains are thus deformed and broken easily under the applied pressure at elevated temperature compared to the β-Al grains with the higher melting point. This can explain the lower roundness and grain size of the η-Zn grains in the thermal-compression microstructure as shown in Figure 8.

As reported by Chen and Tsao [27], four deformation mechanisms have been proposed in the semisolid deformation of nondendritic structures. Liquid flow (LF) and flow of liquid incorporating solid particles (FLS) mechanisms are dominant when the solid particles are surrounded by the liquid phase; plastic deformation of solid particles (PDS) and sliding between solid particles (SS) mechanisms become dominant when the solid particles are in contact with each other [28]. Considering the high volume of solid particles and the irregular geometry as shown in Figure 5(a), the PDS mechanism is dominant initially during the heating period of 380°C to 382°C under pressure. As a result, the deformation of the filler metal is formed by plastic deformation of solid grains. As mentioned above, the η-Zn grains have a lower strength at elevated temperature, resulting from their lower melting point. Therefore, the deformation of the filler metal is formed mainly by plastic deformation of the η-Zn solid grains. By comparing with Figure 5(a), the thickness of the filler metal in the thermal-compression microstructure decreases thus with the deformed η-Zn grains as shown in Figures 7(a_1) and 7(a_2). During the heating period of 382°C to 386°C, both of the β-Al grains and deformed η-Zn grains tend to become spherical, resulting from the recrystallization and the effect of interface curvature. In addition, the β-Al particles with the higher melting point have a higher degree of sphericity than the η-Zn grains as shown in Figure 7(b_1), which leads to the SS mechanism to respond. As a result, the intergranular sliding of the spherical β-Al particles occurs. Along with the intergranular sliding, liquid is expelled towards the free surface of the filler metal. That is why tightly connected grains with less liquid appear in the center of the filler metal, while more liquid are present at the edge of the filler metal as shown in Figures 7(b_1) and 7(b_2). Therefore, the deformation of the filler metal is formed mainly by intergranular sliding of β-Al grains, rarely by deformation of the η-Zn grains and fluidity. The thickness of the filler metal decreases thus with sliding grains, deformed grains, and less fluidity as well. During the heating period of 386°C to 392°C, on the one hand, the η-Zn grains become spheroidized grains of the lowest surface energy. On the other hand, the η-Zn grains are liable to break or fused in the neck shrinkage for a lower free energy. So many near-spherical and small sizes of η-Zn grains can be observed in the filler metal as shown in Figures 7(c_1) and 7(c_2). However, the liquid fraction and the roundness of the β-Al solid grains increase with increasing temperature. The results are consistent with the noncompression microstructure as shown in Figure 5(c). Therefore, the FLS mechanism is activated. That is why the liquid incorporating solid grains can be observed at the edge of the filler metal as shown in Figure 7(c_2). Accordingly, the deformation of the filler metal is achieved mainly by the flow of the liquid incorporating solid grains. The thickness of the filler metal hence decreases with sliding grains and increasing fluidity by comparing with Figure 5(c).When the temperature increases to 410°C, the microstructure consists of coarsen β-Al solid grains with liquid pools as shown in Figure 5(d), and the LF mechanism is hence activated. Due to the nature of the LF mechanism, larger fraction of the liquid is expelled towards the edge. This leads to a high degree segregation of the spheroidal β-Al particles in the center and an amount of fine dendritic grains at the edge as shown in Figures 7(d_1) and 7(d_2). The fine dendritic grains are induced by water quenching

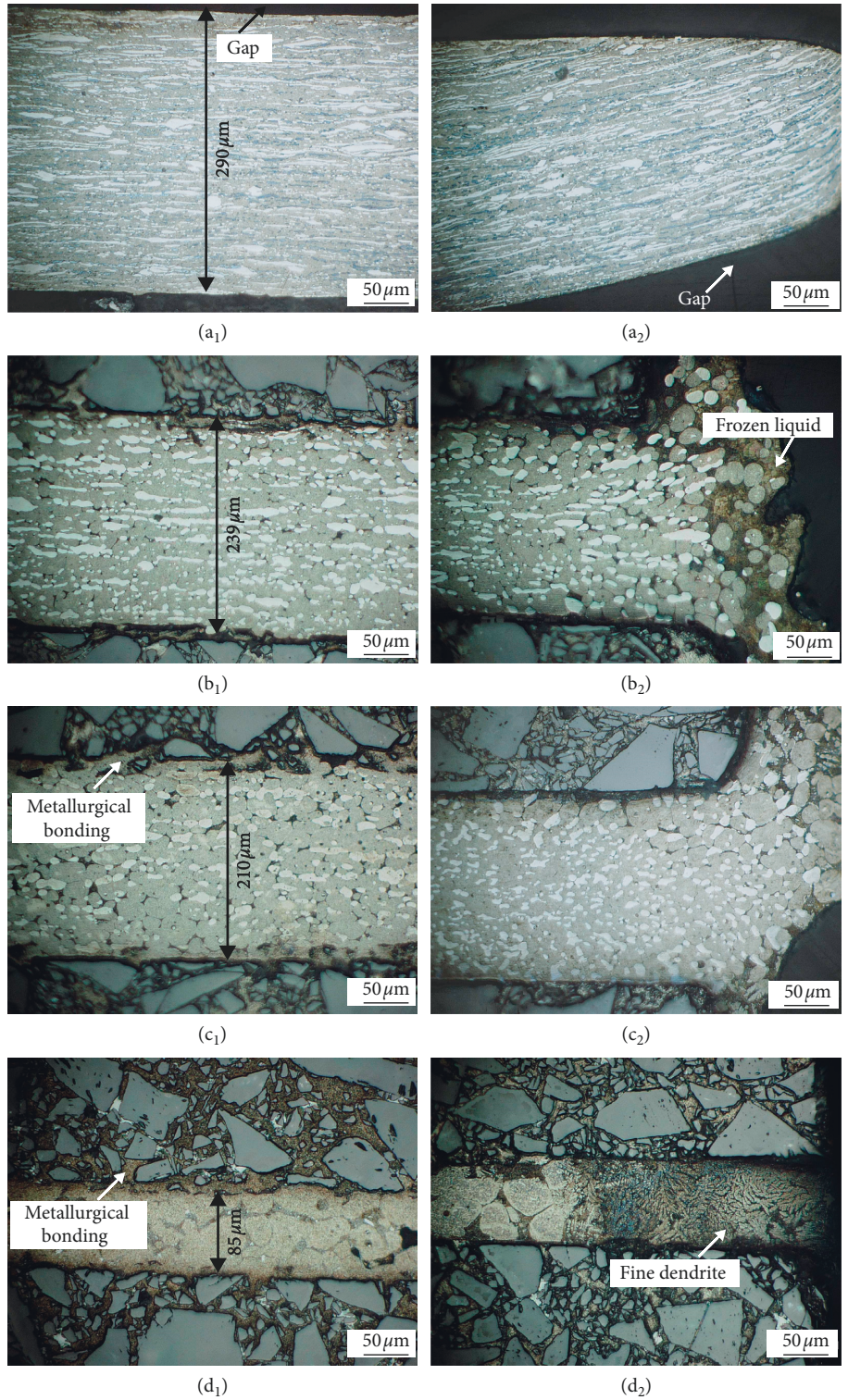

FIGURE 7: The microstructure of the as-rolled filler metal heated to different temperatures with compression between the SiC_p/Al plates: (a_1)–(d_1) center region and (a_2)–(d_2) edge region of the filler metal heated to 382°C, 386°C, 392°C, and 410°C.

of the extrusive liquid. As expected, the deformation of the filler metal is formed by the higher fluidity. The thickness of the filler metal is relatively lower because of the larger fraction of the liquid and higher fluidity.

It is worth highlighting that the increase of the temperature and the disruption of the oxides could aid the diffusion of the Zn-Al-Cu alloy into the base materials. The diffusion will then lower the local melting point and provide

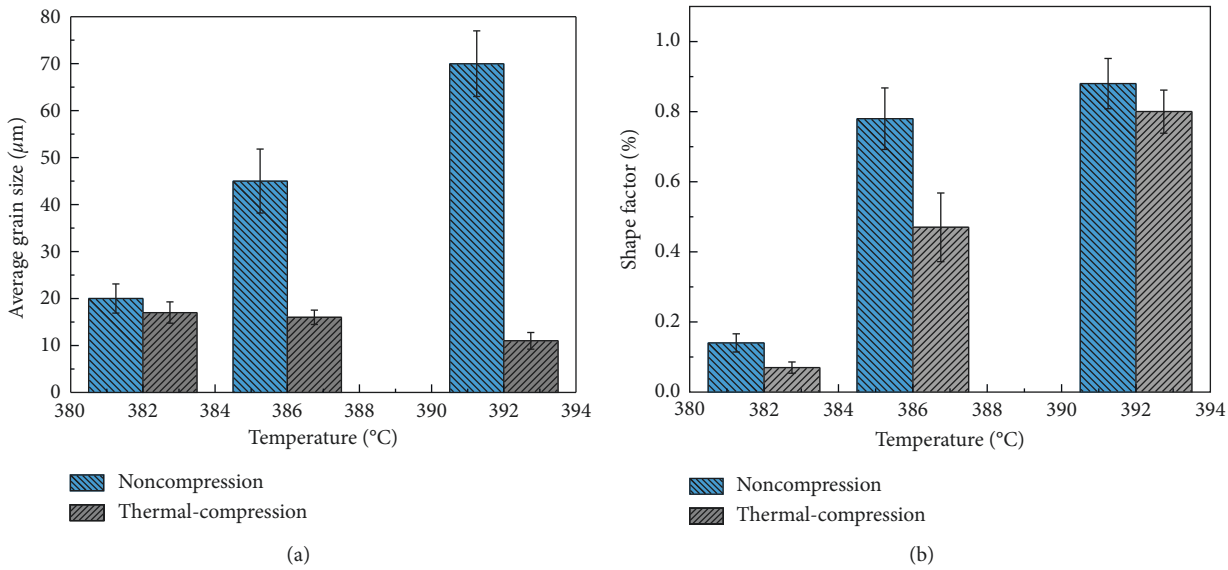

Figure 8: The variation of grain size and shape factor of the η-Zn phase with different microstructures.

a partial melting of the interaction region. As a consequence of cooling, solidification occurs in the interaction region and hence, metallurgical bonding forms.

3.3. Interaction of the Filler Metal with Base Materials on the Interface. Considering the deformation behavior of the filler metal, it can be deduced that the behavior of the filler against the base materials are different during compression. As the PDS mechanism is dominant, the solid grains of the filler metal are deformed under a compressive stress, which, in turn, creates a larger compressive resistance to the interface. So the interaction of the solid grains with base materials at the interface shows an intense compressive stress initially. As reported by Shi et al. [29], the compressive stress will lead to a microplastic deformation to the faying surface. Due to the protruding SiC particles on the surface of the composites, the microplastic deformation is higher with the asperities. When the SS mechanism is dominant, in addition to the compressive stress on the interface, a shear action is exerted by sliding of solid grains and less fluidity of the liquid. The interaction on the interface is thus shear stress and compressive stress. As the FLS mechanism starts to set in, the sliding and fluidity becomes more active. So, the interaction on the interface is higher shear stress combined with compressive stress. Finally, LF becomes dominant. According to the results of Chen and Tsao [27], deformation in this stage is achieved mainly by lateral flow of the liquid. Consequently, the interaction on the interface shows a smaller compressive stress and higher shear stress mainly by fluidity and less by sliding.

3.4. Disruption Mechanism of the Oxide Film. According to the above observations and analysis, the disruption of the oxide film during the brazing process could be divided into four stages. As schematically depicted in Figure 9, when heated from 380°C to 382°C (the first stage), the faying face between the base materials and the filler metal is deformed locally by the compressive stress. Consequently, the continuous oxide films on the faying face crack due to their lower ductility. As the temperature is increased from 382°C to 386°C under pressure (the second stage), the crack extends by substantial compressive stress, and meanwhile, oxide films are scraped as a consequence of the shear stress. With further increase of the temperature (the third stage), more oxide films are broken and stripped away from the faying surface by codominant compressive stress and shear stress. Finally (the last stage), the relative sliding and compressive resistance of the solid grains to the interface diminish, resulting from the larger fraction of the liquid. Therefore, the oxide film on the interface is hard to be broken further with the decreasing compressive and shear stress (Figure 9). In this regard, the heating period of 380°C to 392°C which includes the fore three stages can be considered as an optimum stage for the disruption of the oxide film.

3.5. Mechanical Properties of the Brazed Joint. Figure 10 shows the variation of the shear strength of the joint with the brazing temperature. As shown in Figure 10, the shear strength increases with increasing temperature from 382°C to 392°C and then keeps a constant state value with further increasing temperature. The maximum shear strength reaches 105 MPa which is 78% of the shear strength of the parent material. Figure 11 shows the typical fracture surfaces of the joint brazed at 382°C and 392°C, respectively. A grinding trace with no evidence of bonding is observed at 382°C (Figure 11(a)), while a nonplanar fracture is presented at 392°C as shown in Figure 11(b). The results indicate that, with the effective disruption of the oxide film at 392°C, a sound bonding of the Al matrix and Zn-Al-Cu filler metal is obtained and a high improvement in the shear strength of the joint is achieved.

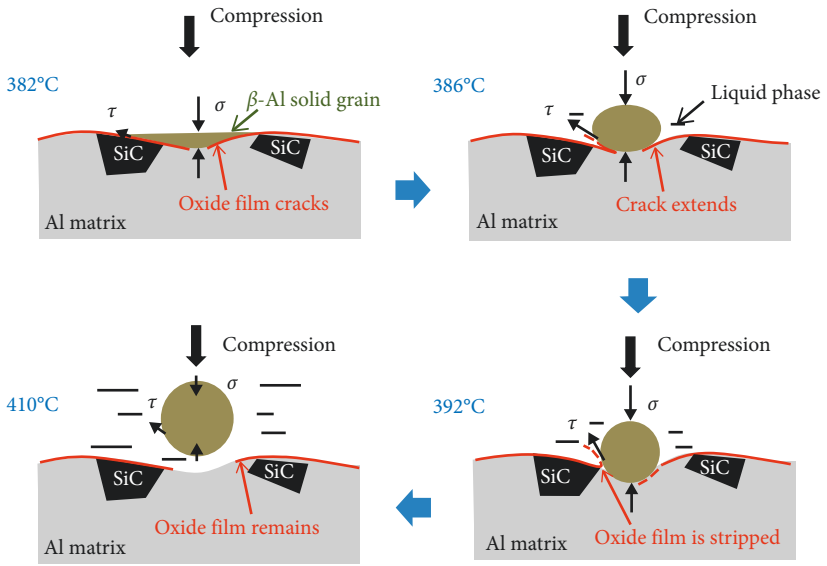

Figure 9: Model of the disruption of the surface oxide film during brazing.

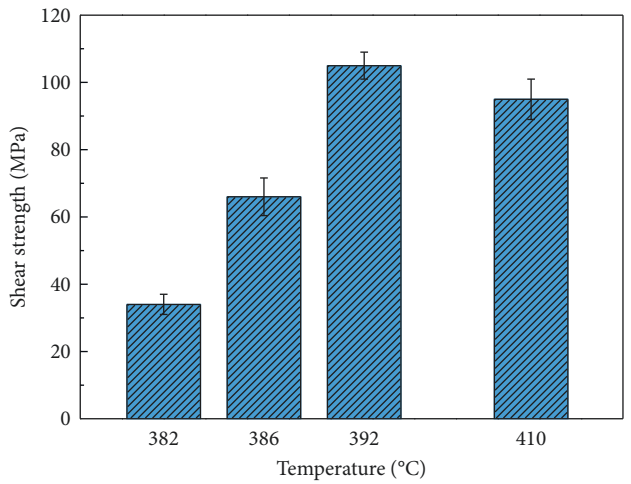

Figure 10: Relationship of shear strength of the joint with the brazing temperature.

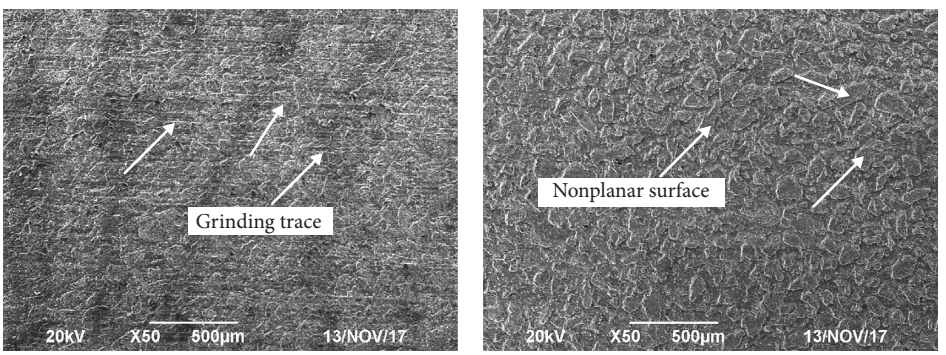

(a) (b)

Figure 11: The fracture surface of the joint brazed at different temperatures: (a) 382°C; (b) 392°C.

4. Conclusions

Semisolid brazing of 63% SiC_p/6063Al composites under an action of applied pressure using Zn-Al-Cu filler metal was performed successfully. The surface oxide film is disrupted sufficiently, and metallurgical bonding is formed.

(1) The microstructure of the filler metal transforms into the semisolid microstructure consisting of globular grains surrounded by liquid after heating treatment. The degree of sphericity and the liquid fraction tend to improve with increasing temperature. Under the applied pressure, the deformation of the filler metal is accomplished by plastic deformation of solid grains when heated to 382°C and then mainly by intergrain sliding and liquid flow with further heating up to 410°C.

(2) Disruption behavior of the surface oxide layer is related to the deformation behavior of the filler metal and the interaction of solid grains to the base material surface during compression. The oxide films are first broken by compressive stress that came from depressing of the solid grains. The oxide films are then stripped away by shear stress which is caused by intergranular sliding of the solid grains and fluidity of the liquid.

(3) After being heated to 392°C under pressure, the surface oxides film can be disrupted significantly and high strength bonds can be obtained. The maximum shear strength of the brazed joints reached 105 MPa. This achieves 78% of the shear strength of the parent material (135 MPa).

Data Availability

The data used to support the findings of this study are included within the article.

Conflicts of Interest

The authors declare that there are no conflicts of interest regarding the publication of this paper.

Acknowledgments

This project was supported by the National Natural Science Foundation of China (No. 51435004).

References

[1] A. Urena, L. Gil, E. Escriche, J.-M. G. de Salazar, and M.-D. Escalera, "High temperature soldering of SiC particulate aluminum matrix composites (series 2000) using Zn-Al filler alloys," *Science and Technology of Welding and Joining*, vol. 6, no. 1, pp. 1–11, 2001.

[2] X.-P. Zhang, G.-F. Quan, and W. Wei, "Preliminary investigation on joining performance of SiCp-reinforced aluminum metal matrix composite (Al/SiCp-MMC) by vacuum brazing," *Composites Part A: Applied Science and Manufacturing*, vol. 30, no. 6, pp. 823–827, 2009.

[3] Z.-W. Xu, L. Ma, J.-C. Yan, S.-Q. Yang, and S.-Y. Du, "Wetting and oxidation during ultrasonic soldering of an alumina reinforced aluminum-copper-magnesium (2024 Al) matrix composite," *Composites Part A: Applied Science and Manufacturing*, vol. 43, no. 3, pp. 407–414, 2012.

[4] L. Ma, Z.-W. Xu, K. Zheng, J.-C. Yan, and S.-Q. Yang, "Vibration characteristics of aluminum surface subjected to ultrasonic waves and their effect on wetting behavior of solder droplets," *Ultrasonics*, vol. 54, no. 3, pp. 929–937, 2014.

[5] Q. Wang, X.-G. Chen, L. Zhu et al., "Rapid ultrasound-induced transient-liquid-phase bonding of Al-50Si alloys with Zn interlayer in air for electrical packaging application," *Ultrasonics Sonochemistry*, vol. 34, pp. 947–952, 2017.

[6] L. Zhu, Q. Wang, L. Shi et al., "Ultrarapid formation of multi-phase reinforced joints of hypereutectic Al-Si alloys via an ultrasound-induced liquid phase method using Sn-51In interlayer," *Materials Science and Engineering A*, vol. 711, pp. 94–98, 2018.

[7] X.-G. Chen, J.-C. Yan, F. Gao, J.-H. Wei, Z.-W. Xu, and G.-H. Fan, "Interaction behaviors at the interface between liquid Al-Si and solid Ti-6Al-4V in ultrasonic-assisted brazing in air," *Ultrasonics Sonochemistry*, vol. 20, no. 1, pp. 144–154, 2013.

[8] Z. Huiwen, C. Wei, H. Jingshan, Y. Jiuchun, and Y. Shiqin, "Formation and evolution of intermetallic compounds at interfaces of Cu/Al joints by ultrasonic-assisted soldering," *Journal of Materials Processing Technology*, vol. 223, pp. 1–7, 2015.

[9] W.-B. Guo, T.-M. Luan, J.-S. He, and J.-C. Yan, "Ultrasonic-assisted soldering of fine-grained 7034 aluminum alloys using ZnAl filler metals," *Materials and Design*, vol. 125, pp. 85–93, 2017.

[10] T. Watanabe, K. Noguchi, A. Yanagisawa, and S. Satoh, "Soldering of aluminum with the aid of ultrasonic vibration (5th Report). The effect of ultrasonic vibration on soldering Al-Mg alloy," *Quarterly Journal of the Japan Welding Society*, vol. 14, pp. 260–266, 1996.

[11] S. Sugiyama, M. Kiuchi, and J. Yanagimoto, "Application of semisolid joining—Part 4 glass/metal, plastic/metal, or wood/metal joining," *Journal of Materials Processing Technology*, vol. 201, no. 1–3, pp. 623–628, 2008.

[12] Y.-S. Cheng and X.-H. Zhang, "Interfacial strength and structure of joining between 2024 aluminum alloy and SiC_p/2024 Al composite in semi-solid state," *Materials and Design*, vol. 65, pp. 7–11, 2015.

[13] A. Narimannezhad, H. Aashuri, A.-H. Kokabi, and A. Khosravani, "Microstructural evolution and mechanical properties of semisolid stir welded zinc AG40A die cast alloy," *Journal of Materials Processing Technology*, vol. 209, no. 8, pp. 4112–4121, 2009.

[14] V.-A. Hosseini, H. Aashuri, and A.-H. Kokabi, "Mechanisms of joint formation throughout semisolid stir welding of AZ91 magnesium alloy," *Transactions of Nonferrous Metals Society of China*, vol. 23, no. 9, pp. 2585–2590, 2013.

[15] V.-A. Hosseini, H. Aashuri, and A.-H. Kokabi, "Characterization of newly developed semisolid stir welding method for AZ91 magnesium alloy by using Mg-25% Zn interlayer," *Materials Science and Engineering A*, vol. 565, pp. 165–171, 2013.

[16] J.-C. Yan, H.-B. Xu, L. Shi, X.-L. Wang, and S.-Q. Yang, "Vibration assisted brazing of SiCp/A356 composites: microstructure and mechanical behavior," *Science and Technology of Welding and Joining*, vol. 13, no. 8, pp. 760–764, 2008.

[17] H.-B. Xu, Q.-X. Xing, Y.-L. Zeng, Y. Luo, and C.-H. Du, "Semisolid stirring brazing of SiC_p/A356 composites with Zn27Al filler metal in air," *Science and Technology of Welding and Joining*, vol. 16, no. 6, pp. 483–487, 2011.

[18] H.-B. Xu, B.-F. Zhou, C.-H. Du, Q.-X. Luo, and H.-Y. Chen, "Microstructure and properties of joint interface of semisolid stirring brazing of composites," *Journal of Materials Science and Technology*, vol. 28, no. 12, pp. 1163–1168, 2012.

[19] H.-B. Xu, Q.-X. Luo, B.-F. Zhou, Y.-L. Zeng, and C.-H. Du, "The effect of stirring rate on semisolid stirring brazing of SiC_p/A356 composites in air," *Materials and Design*, vol. 34, pp. 452–458, 2012.

[20] S.-M. J. Alvani, H. Aashuri, A. Kokabi, and R. Beygi, "Semisolid joining of aluminum A356 alloy by partial remelting and mechanical stirring," *Transactions of Nonferrous Metals Society of China*, vol. 20, no. 9, pp. 1792–1798, 2010.

[21] T. Savaşkan and A.-P. Hekimoğlu, "Microstructure and mechanical properties of Zn–15Al-based ternary and quaternary alloys," *Materials Science and Engineering A*, vol. 603, pp. 52–57, 2014.

[22] A. Bolouri, M. Shahmiri, and E.-N. H. Cheshmeh, "Microstructural evolution during semisolid state strain induced melt activation process of aluminum 7075 alloy," *Transactions of Nonferrous Metals Society of China*, vol. 20, no. 9, pp. 1663–1671, 2010.

[23] E. Parshizfard and S.-G. Shabestari, "An investigation on the microstructural evolution and mechanical properties of A380 aluminum alloy during SIMA process," *Journal of Alloys and Compounds*, vol. 509, no. 40, pp. 9654–9658, 2011.

[24] L. P. Wang, W.-Y. Jiang, T. Chen et al., "Spheroidal microstructure formation and thixoforming of AM60B magnesium alloy prepared by SIMA process," *Transactions of Nonferrous Metals Society of China*, vol. 22, pp. 435–444, 2012.

[25] B. Behzad and A.-K. Mehrdad, "Phase evolution and mechanical behavior of the semi-solid SIMA processed 7075 aluminum alloy," *Metals*, vol. 6, no. 3, pp. 1–23, 2016.

[26] T.-A. Witten and L.-M. Sander, "Diffusion-limited aggregation, a kinetic critical phenomenon," *Physical Review Letter*, vol. 47, no. 19, pp. 1400–1408, 1981.

[27] C.-P. Chen and C.-Y. A. Tsao, "Semi-solid deformation of non-dendritic structures-I. Phenomenological behavior," *Acta Metallurgica*, vol. 45, no. 5, pp. 1955–1968, 1997.

[28] C.-P. Chen and C.-Y. A. Tsao, "Semisolid deformation of aluminium alloy 356 with non-dendritic structure," *Materials Science and Technology*, vol. 15, no. 9, pp. 981–985, 1999.

[29] L. Shi, J.-C. Yan, Y.-F. Han, and B. Peng, "Behaviors of oxide layer at interface between semi-solid filler metal and aluminum matrix composites during vibration," *Journal of Materials Science and Technology*, vol. 27, no. 8, pp. 746–752, 2011.